

CornerFormer: Boosting Corner Representation for Fine-Grained Structured Reconstruction

Hongbo Tian^{1, 2 *} Yulong Li^{2*} Linzhi Huang^{1, 2} Yue Yang² Xiangang Li²

Weihong Deng^{1 †}

¹Beijing University of Posts and Telecommunications, ²Beike

{tianhongbo, huanglinzhi, whdeng}@bupt.edu.cn

{liyulong008, yangyue092, lixiangang002}@ke.com

April 21, 2023

Abstract

Structured reconstruction is a non-trivial dense prediction problem, which extracts structural information (*e.g.*, building corners and edges) from a raster image, then reconstructs it to a 2D planar graph accordingly. Compared with common segmentation or detection problems, it significantly relies on the capability that leveraging holistic geometric information for structural reasoning. Current transformer-based approaches tackle this challenging problem in a two-stage manner, which detect corners in the first model and classify the proposed edges (corner-pairs) in the second model. However, they separate two-stage into different models and only share the backbone encoder. Unlike the existing modeling strategies, we present an enhanced corner representation method: 1) It fuses knowledge between the corner detection and edge prediction by sharing feature in different granularity; 2) Corner candidates are proposed in four heatmap channels w.r.t its direction. Both qualitative and quantitative evaluations demonstrate that our proposed method can better reconstruct fine-grained structures, such as adjacent corners and tiny edges. Consequently, it outperforms the state-of-the-

art model by +1.9%@F-1 on Corner and +3.0%@F-1 on Edge.

1 Introduction

Structured reconstruction[2, 9, 8] is a fundamental task for rendering, effects mapping, human-computer interaction, etc. It requires a thorough understanding of the geometrical information in the image and then represents it in vector form, such as CAD format.

In recent years, computer vision-based structured reconstruction has proven successful for the reconstruction of interior floor plans [25],[6]. While the outdoor structured reconstruction is still challenging, owing to its sophisticated structure. It suffers from dense targets (*e.g.*, redundant non-target structures, adjacent corners or tiny edges in Fig. 1), which may lead to the collapse of the whole reconstruction. Human vision goes beyond computers in structured reconstruction not only in the understanding of the overall structure but also in the local fine-grained structure. Inspired by the strengths of human perceptual capability, we propose an improvement method introduced briefly in Fig. 1 for the current advanced work.

At first, the reasoning process of humans on structure information requires global and local coordination. During perceiving corners, we have a basic

*This work was done when the authors were visiting Beike as interns.

[†]Corresponding author.

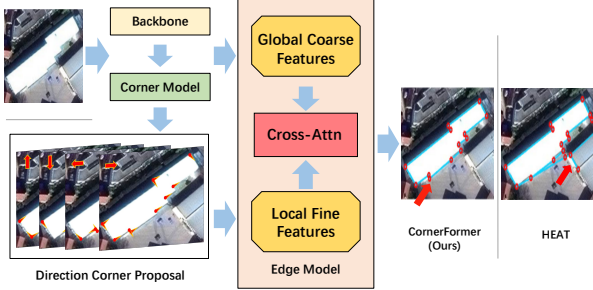


Figure 1: **The basic idea of CornerFormer.** Red arrows indicate non-target structures and tiny edges. CornerFormer perceives both the global information and the local fine grained information.

understanding of high-level semantics, like edges and regions. Therefore, Corner detection and edge prediction are inseparable in such a reasoning process [29], [30]. However, the current advanced methods ignore such phenomenon [32], [7]. They treat corner detection and edge prediction as two detachable modules, which can be employed alone. It results in a severe loss of local information. This is inconsistent with human cognitive processes.

Our method leverages corner detection to assist edge prediction by treating the feature proposal as the anchor of query embedding [38]. Specifically, the fine-grained structural semantics is learned from local fine features according to the proposed corners, and the high-level geometric construction is learned from global coarse features [7].

The other problem in the current methods is the quantization error [16] caused by corner detection [7, 36, 24]. Adjacent corners at a very close distance will be mixed up after the non-maximum suppression (NMS). In response to this problem, we designed the direction corner module to learn the corner according to its direction, which greatly alleviated the problem of adjacent corners and boosted corner representation.

Our method effectively compensates for the information loss between corner detection and edge prediction and is more sensitive to fine structures. We evaluate the proposed method in outdoor architecture recon-

struction [22] from satellite images and it performs well especially in the corner and edge scores. The contributions of our method can be summarised as follows:

- 1) Fine-grained image features based on the corner proposal are used to assist edge prediction without the increase of parameters. Besides, a proposal feature enhancement module (PFEM) is designed to facilitate the convergence of fine features.
- 2) A direction corner module is adopted for tiny edges in structured reconstruction to solve adjacent corners problem and to boost corner representation.
- 3) Our work is proved to outperform the current competing methods in outdoor building architecture with complex environments through quantitative and qualitative experiments.

2 Related Work

2.1 Structured Reconstruction

We introduce structured reconstruction work based on two different structure inference processes. One is top-down method, and the other is bottom-up method. The top-down method is based on the fact that the structure is a simple 1D polygonal loop [1, 5, 3]. This method employs an instance segmentation algorithm such as Mask R-CNN [10] for room proposal, and then iteratively optimizes the proposed rooms. Specifically, FloorSP [6] and Cabral *et al.* [3] explore the shortest path algorithm to reconstruct an indoor floorplan. MonteFloor [25] based on Monte Carlo Tree Search maximizes a suitable objective function for planar graphs. However, these methods do not perform well in complex outdoor environments with nested loops and the outdoor structured reconstruction mainly adopts the method of bottom-up [22, 35, 12]. IP [22] and Exp-clis [33] based on heuristics extract structural information and infer the graph structure. They are powerful but require the design of rigorous rules for extensive optimization and search process. Con-vMPN [32] and HEAT [7] sought solutions without

structural optimization by directly fusing line segment information into image features.

Structure inference based on bottom-up relies heavily on the results of corner detection, while current advanced methods [32, 30] all design a detachable module to better focus on the improvement of piecewise results. Our model can combine the two-stage models to improve the two-stage performance synchronously.

2.2 Vision Transformer

Transformer [27] already has a capacity in computer vision that matches and even surpasses convolutional neural networks. It has the entire receptive field of a feature map. For the same reason, even the transformer model adopted by DETR [4] shows strong performance in the object detection task, but the memory access sharply increases with the feature scale and the computational complexity grows quadratically with the spatial size. Deformable-DETR [39] adaptively learns the feature in limited locations from the feature maps and Feature Pyramid Networks(FPN) divides the features into different levels to alleviate the problem. Both above can effectively reduce the computational burden of the model but are difficult to converge during training by using a dummy query [29, 4]. Improvement schemes [18, 20, 34] based on DETR turn out that the initialization of anchors makes the transformer model converge easily. This paper directly takes the anchor feature from the corner model as the input of the edge prediction and further introduces the feature information of corner detection. By boosting the corner representation, our method accelerates the convergence of query embedding and performs well in optimizing corner proposal.

2.3 Adjacent Corners Problem

Both human detection and wireframe parsing tasks based on the bottom-up method need to detect corner primitives first. The traditional methods [26, 28, 31] detect corners based on heatmap followed by NMS, but can not avoid quantization errors caused by NMS. Some classic work based on the regression [15, 19, 16] solves the problem. Wireframe parsing methods

[13], [36] alleviate this problem through patches of heatmap and regression. IP [22] and DWP [37] perform a fine-grained design of corner bins according to the angle. Besides, R2V [17] scatters different corners into different channels according to their types, which also avoids part of the problem.

Our direction corner detection is inspired by characteristics of corners [21], [17].

In outdoor structure reconstruction, most of the adjacent corners will form tiny edges. We scatter the tiny edge endpoints into different channels according to the directions of the two endpoints of an edge to complete the detection of tiny edges.

3 Method

We have shown the complete network system in Fig. 2 and we will explain our model in six sections. 1) The preliminaries in our method; 2) Corner detection with the corner decoder and direction corner proposal; 3) Learnable corner feature extractor to extract corner features according to proposed corners; 4) Proposal feature enhancement module; 5) Edge decoder for edge prediction; and 6) Loss function.

3.1 Preliminaries

Pipeline. Corner detection is responsible for corner proposal and the proposed corners are grouped in pairs considered as candidate edges. During training, we take all GT edges as well as the wrong candidate edges (randomly combined based on the predicted corners and supplementary materials for details) to generate our candidate set. The maximum number of candidate edges in the candidate set is T , and all the candidate edges in our set are delivered to the edge prediction for holistic prediction. In the inference process, all the proposed corners n are freely combined into C_2^n candidate edges for edge prediction. Finally, our model is evaluated based on the precision/recall/F-1 scores of the corner/edge/region primitives.

Data preparation. The main notations go first to make our method more intuitive. The input is the cropped satellite image $I \in \mathbb{R}^{H,W,3}$. Extracted coarse features and fine features are represented as F_{coarse}

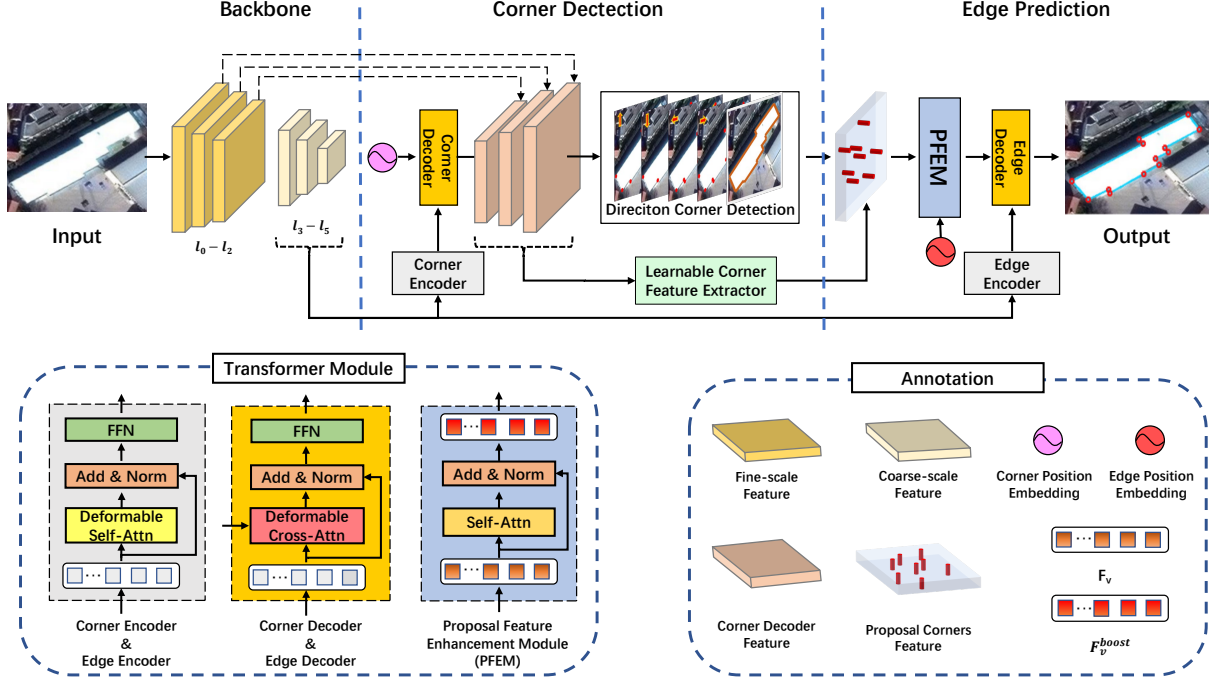


Figure 2: **CornerFormer Architecture.** Coarse-scale feature maps $l_3 - l_5$ are assigned to the encoder for extracting **global coarse features**. Fine-scale feature maps $l_0 - l_2$ are assigned to the corner decoder for direction corner detection. The proposed corner features (red cylinders) are extracted by a learnable corner feature extractor. Proposal feature enhancement module (PFEM) is designed to boost the proposed feature F_v and learns **local fine features**.

and F_{fine} respectively. For all the quantization results, we denote the proposal corner as \mathbf{e} , and the coordinate corresponding to the current corner is denoted as (x, y) . A candidate edge grouped by pair corners is denoted as \mathbf{v} . A weight learned through a layer of linear mapping is denoted as W . For any one of the proposed corners, we extract corner feature $\Phi = \{\phi_l\}_{l=0}^L$. L denotes the total number of feature layers from corner decoder feature maps. A set of candidate edge features is represented by $F_v = \{f_v^t\}_{t=1}^T$. An individual edge proposal feature f_v formed from coupled Φ .

Backbone. The backbone is based on Resnet [11] and the stacked convolutional layers from a multi-scale feature pyramid. The 6-layers feature maps is corresponding to six different scales $F^l \in \mathbb{R}^{\frac{H}{2^l}, \frac{W}{2^l}, C^l}$, ($l =$

$0, 1, \dots, 5$). Coarse-scale feature maps $l_3 - l_5$ are assigned to the encoder for extracting global coarse features. Fine-scale feature maps $l_0 - l_2$ are assigned to the corner decoder for corner detection. This is accord with HEAT [7].

Image encoder. To ensure the computation cost is acceptable, a multi-scale transformer encoder requires compressing large scale feature maps into a small size. Hence, the coarse-scale feature maps $l_3 - l_5$ from the backbone are assigned for self-attention encoding. Both corner model and edge model employ the same encoder from deformable-DETR [39] for corner detection and edge prediction respectively. The key and query elements in transformer are pixels from the coarse-scale feature maps which are flattened to query embedding $\mathbf{q} \in \sum_{l=3}^5 \frac{H \cdot W}{2^{2l}}, C$. At the same time, the

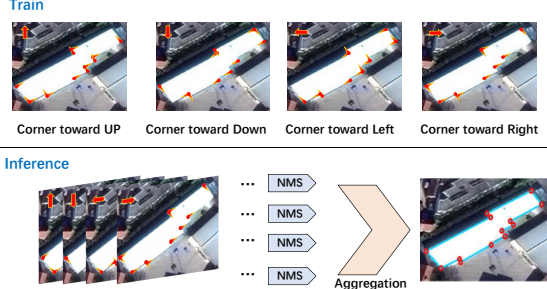


Figure 3: **Direction corner module** for train and inference. The direction of the arrow indicates the orientation of the corners.

central reference point and position encoding are provided for each feature map, which effectively reduces the computational complexity compared to DETR-style transformer encoder [4].

3.2 Corner detection

Corner decoder. Based on the consensus that there exists only one corner within the 4×4 pixel patch, one layer of corner decoder was employed to decode all position embedding of 4×4 patches in an image. The output from the corner decoder is mixed with the backbone at fine-scale ones, $l_0 - l_2$. This process is similar to matching the stacked hourglass network [23] with the transformer system. The output feature map from corner decoder is concatenated with the corresponding scale feature map from the backbone respectively by convolution and upsampling. We transform all the fine-scale feature maps to 128-dimensions for proposal feature extraction in Sec. 3.3.

Direction corner module. In outdoor structure reconstruction, there are lots of tiny edges with adjacent corners. Inspired by the work of GANet [21], the tiny edge endpoints detected by the corner detection can be scattered into different channels according to the directions of the two endpoints of an edge.

Specifically (See Fig. 3), in the training process, we classify all corners into four categories according to the direction of the edge on the structure. It brings corners with different semantic directions (up,

down, left, right). Then, the loss function L_{direct} is assembled to learn them onto four confidence maps $Y \in \mathbb{R}^{H,W,4}$, using a Gaussian blur $G(x, y)$ as follows:

$$G(x, y) = \frac{1}{2\pi\sigma^2} \exp\left(-\frac{(x - \tilde{x})^2 + (y - \tilde{y})^2}{2\sigma^2}\right) \quad (1)$$

where \tilde{x} and \tilde{y} denote the corners with directional semantics and σ is the standard deviation depends on the gaussian kernel. An additional line segment semantic segmentation loss L_{seg} is used to supervise direction corner learning. During inference, we perform non-maximum suppression (MNS) on the predicted confidence maps with different semantic corners, respectively. All the corners whose cluster centroid distance is less than L are clustered, where $L=5$.

Because any pair of corners from the same edge has completely opposite semantics (such as top and bottom), all proposed corners can be represented after the corner aggregation. However, this approach does not solve the problem of adjacent corners on the same horizontal line when the direction of GT corner toward the left and the right can not be separated in the up-to-down corner channel. The four direction channels boost the corner representation and complement the prediction to guarantee that all the adjacent corners are independent in a certain direction corner prediction channel.

3.3 Learnable corner feature extractor

Using guidance like learnable position encoding effectively improves the decoding performance of transformer [7]. We further propose the local fine features from corner model according to the proposed corners. The corner feature $\phi^l(x, y)$ is given by

$$\phi^l(x, y) = F_{fine}^l\left(\frac{x}{2^l}, \frac{y}{2^l}\right) \quad (2)$$

where $l = 0, 1, 2$ and F_{fine}^l is the fine features corresponding to the three scales from corner decoder feature. A learnable weight matrix A_e can adaptively focus on proposed corners from different scale feature maps.

$$A_e = \text{softmax}(\Phi(x, y) \cdot W_e) \quad (3)$$

$$f_e = \sum_{l=0}^2 A_e^l \phi^l(x, y) \quad (4)$$

A_e is learned from $\Phi(x, y)$ based on a linear layer followed by softmax. $\Phi \in \mathbb{R}^{3 \times 128}$ represents the fine features concatenated by $\phi(x, y)$. f_e is the corner feature normalized based on weights feature-wise.

If the learned different channel weights are all 1 for one of the layers, our approach is equivalent to using features only in that layer as our proposal corner feature.

3.4 Proposal feature enhancement module

Pairs of corner features are linearly mapped to represent proposal edge feature $f_v = W_v(f_{e_1}; f_{e_2})$. It is valid to decode proposal edge feature directly, but the effect is not significant according to Sec. 4.3. Our hypothesis is that due to the difficulty of query convergence [4, 38], the model will be more inclined to obtain image information from global coarse-scale features. In order to facilitate query convergence and extract fine-grained image features in query, proposal feature enhancement module (PFEM) is designed.

At first, a learnable cosine encoding is borrowed from HEAT [7] as the position embedding f_v^{pos} .

$$f_v^{pos} = W_v^{pos}(\theta_{e_1}; \theta_{e_2}) \quad (5)$$

where θ is cosine encoding of the corner coordinates [27]. PFEM employs a 6-layers self-attention module of transformer to boost the proposal feature F_v , whose general formula is:

$$F_{self} = \sum_{m=1}^M W_m [\text{softmax}(\frac{QK}{\sqrt{d}})V] \quad (6)$$

$$F_v^{boost} = \text{Add\&Norm}(F_v, F_{self}) \quad (7)$$

where $Q = (F_v + F_v^{pos})W_Q$, $K = (F_v + F_v^{pos})W_K$, and $V = F_vW_V$. F_{self} is the output of the self-attention layer. F_v^{boost} is boosted candidate proposal feature. M denotes the number of attention self-attention heads and $M = 8$ for ours. Finally, a feed-forward network (FFN) is used to integrate information and learn fine-grained features on fine-scale feature maps.

3.5 Edge decoder

The edge decoder is also 6-layers in total and deformable cross-attention module is adopted to obtain global coarse features from coarse-scale feature maps. Each candidate edge boosted f_v^{boost} will query the S location features noticed in global coarse features F_{coarse} . The complete formula for the output of D-Cross Attention F_{cross} in Fig. 2 is expressed as:

$$F_{cross} = \sum_{l=3}^5 \sum_{s=1}^S A(v)_{ls}^{boost} F_{coarse}^l [p_{lv} + \Delta_{ls}(f_v^{boost})] \quad (8)$$

where a linear projection layer is used to learn the corresponding attention position $\Delta(f_v^{boost})$ and attention weight $A(v)^{boost}$. The initialized attention position p is the center point of the candidate edge to accelerate the query of the S location. The same FFN layer shared weights by the proposal feature extraction module is employed to learn the feature F_{edge} :

$$F_{edge} = \text{FFN}(\text{Add\&Norm}(F_v^{boost}, F_{cross})) \quad (9)$$

F_{edge} is eventually used to predict the candidate edges. We compare the cross-attention module from DETR [4] with deformable cross-attention module in our work. Referring to Sec. 4.3, deformable cross-attention with $S = 4$ is applicable to our work.

3.6 Loss function

The final loss function consists of four branches and binary cross entropy (BCE) loss is adopted for all four losses. The total loss function is:

$$Loss = \lambda_1 L_{direct} + \lambda_2 L_{seg} + L_{boost} + L_{edge} \quad (10)$$

1) **Direction Corner Loss** is used to detect different semantic corners in confidence feature maps. 2) **Segmentation Loss** performs semantic segmentation of line segments to assist direction corner detection. 3) **Boosting Loss** supervises proposal features F_v^{boost} which facilitate query convergence and extract fine-grained image features. 4) **Edge Loss** is employed to predict edge based on F_{edge} by the shared FFN. λ_1 and λ_2 are the given hyper-parameter to balance the weights.

4 Experiments

Experiment details: We implemented the proposed method in PyTorch. The learning rate is initialized to $2e-4$, which decreases to $1e-5$ at 600 epochs with a total of 800 epochs consistent with the previous work [7]. We train our model with a batch size of 32 for the image size 256×256 and a batch size of 12 for the image size 512×512 by using the Adam optimizer [14]. All the experiments are done in dual Tesla V100 GPUs. Both loss weight λ_1 and λ_2 are set as 0.05. We set the maximum number of training maximum candidate edges to $T = 800$ to ensure that all the candidate edges fully participate in the training. All candidate edges participate in the prediction during inference.

Dataset: Outdoor architecture reconstruction is a building vectorization dataset proposed by Nauata et al. [22], which leverages to solve the architecture vectorization problems. The input is a satellite RGB image from either Paris, Las Vegas or Atlanta and the output is a planar graph depicting both the internal and external architectural edges in the roof of buildings. The dataset contains 2001 satellite images in total and 1601, 50, 350 for training, validation, testing, respectively. The precision/recall/F-1 scores of the corner/edge/region primitives are the metrics of the dataset. Outdoor architecture reconstruction is a challenging problem for computer vision because it’s not just about learning corner connections similar to floorplan vectorization and further needs to distinguish the target building structure and the edge segments with other semantics (*e.g.*, shadows, lawns, and non-target structures).

4.1 Competing methods

We conduct comparative evaluations against with six competing methods: IP [22], ConvMPN [32], Expcls [33], HAWP [30], LETR [29], HEAT [7]. The methods are introduced briefly as follows:

- **IP** leverages integer programming algorithm to integrate detected primitives (*e.g.*, corners, edges) and their related information into a planar graph. This is the first SOTA algorithm for the current dataset.

- **ConvMPN** is based on an improved graph neural network in which nodes correspond to building edges in an image. This is a single structure detection model for the proposed corners.

- **Exp-cls** optimizes the proposed structure from the baseline model (*e.g.*, IP, Conv-MPN) through iterative exploration and classification. The computational framework is general but expensive compared to the end-to-end system.

- **HAWP** combines Attraction Field Map (AFM) representation method to pre-filter candidate edges. It predicts edges based on the corner feature map without global features.

- **LETR** is an end-to-end wireframe parsing algorithm based on transformer framework. It inherits the advantages of DETR [4] and works end-to-end without edge, connection, region detection, and heuristic guidance.

- **HEAT** is the current SOTA which designs an end-to-end network system with independent corner detection and edge prediction. Our method builds on this to perform the overall learning of corner detection and edge prediction through feature transfer.

Comparisons of all the competing methods are based on publicly available data in original papers. In particular, for HAWP and LETR which do not carry official results in the current dataset, we borrow the results from HEAT based on official implementations.

4.2 Evaluation

Quantitative evaluation: Table 1 presents the quantitative evaluation with competing methods. Our Method CornerFormer in outdoor architecture reconstruction achieved the SOTA. Our method focuses more on the attention of all candidate edges. In order to realize the direct transfer of boosting corner representation, CornerFormer abandons the filtering edge candidates in HEAT and leverages more resources to realize the two-stage information synchronization.

When the proportion of memory access is the same, the number of parameters for our model (46.97M) is relatively lower than HEAT (48.94M). In terms of inference speed, we can exceed the performance from HEAT with three times inference by only one simple

Table 1: **Quantitative evaluations on outdoor architecture reconstruction.** Size: the size of the input image. End-to-end: a complete end-to-end neural system for both corner proposal and edge prediction. The colors **cyan** and **orange** mark the top-two results with different image sizes.

Evaluation Type			Corner			Edge			Region		
Method	Size	End-to-end	Prec	Recall	F-1	Prec	Recall	F-1	Prec	Recall	F-1
IP [22]	256	-	-	-	74.5	-	-	53.1	-	-	55.7
ConvMPN [32]	256	-	78.0	79.7	78.8	57.0	59.7	58.1	52.4	56.5	54.4
Exp-Cls [33]	256	-	92.2	75.9	83.2	75.4	60.4	67.1	74.9	54.7	63.5
HAWP [30]	256	✓	90.9	81.2	85.7	76.6	68.1	72.1	74.1	55.4	63.4
LETR [29]	256	✓	87.8	74.8	80.8	59.7	58.6	59.1	68.3	48.7	56.8
HEAT [7]	256	✓	91.7	83.0	87.1	80.6	72.3	76.2	76.4	65.6	70.6
CornerFormer(Ours)	256	✓	94.1	84.5	89.0	83.8	75.1	79.2	77.8	66.9	71.9
HAWP [30]	512	✓	90.6	83.7	87.0	78.8	72.0	75.2	77.5	57.8	66.2
LETR [29]	512	✓	90.3	79.7	84.7	64.0	71.6	67.6	77.1	62.6	69.1
HEAT [7]	512	✓	90.7	86.7	88.7	82.2	77.4	79.7	79.6	69.0	73.9
CornerFormer(Ours)	512	✓	92.6	87.8	90.2	83.3	79.4	81.3	79.4	72.8	76.0

inference With the help of the structure information transferred from the corner detection. The inference speed is more than twice as fast as the current SOTA, and much faster than heuristic methods, such as IP and Exp-cl. The default image size of the dataset is 256×256. In order to compare with HAWP, LETR, and others, we resize the image to 512×512 for train and evaluation. Quantitative experiments show that our method has a more significant improvement in region recall, which can recall smaller target regions.

Qualitative evaluation: For the task of fine-grained structured reconstruction which needs to pay more attention to the detection of "structural corners", ConerFormer shows the extreme advantage in corner proposal. After our feature boosting, more fine-grained corners are detected to assist edge prediction. Many invalid corners of the graph are filtered out (*e.g.*, invalid structures inside the detected target, as well as non-detected objects) compared to competing methods.

In general, we make a great improvement in maintaining the consistency of the two-stage model and perceiving fine-grained structure, which is particularly important for the vectorization problem of satellite images with complex environments and dense corners.

4.3 Ablation studies

Table 2: **The ablation of different components designed in our edge prediction.** The evaluation metric is the scores of corner/edge/region F-1. CER denotes the candidate edge representation which applies endpoints (EP) or center-point (CP). CN and DCN denote vanilla convolution and deformable convolution in corner feature extractor. SA, CA, and DCA denote the self-attention layer from PFEM, cross-attention layer, and deformable cross-attention layer from edge decoder.

CER		Convolution		Transformer			Evaluation		
EP	CP	CN	DCN	SA	CA	DCA	Corner	Edge	Region
✓		✓			✓		86.9	74.9	58.3
✓		✓				✓	87.0	75.6	66.2
	✓	✓		✓			87.2	75.3	67.0
✓		✓		✓			87.5	76.2	69.5
✓		✓		✓	✓		87.6	77.0	67.9
✓		✓		✓		✓	87.7	76.9	70.8
✓			✓	✓		✓	87.9	77.4	70.7

Horizontal ablation experiments: We investigate the effect of different components designed in our edge



Figure 4: **Qualitative evaluations on outdoor architecture reconstruction** with image size 256×256 . Our models provide better perception of fine structures, especially corners.

prediction model horizontally in Table 2. We contrast the representations of different candidate edges, the **endpoints** and the **center-point**, as the candidate

edge features. Center-point representation is inspired by CenterFormer [38] with the predicted center-point of the candidate edges. Experiment results show that

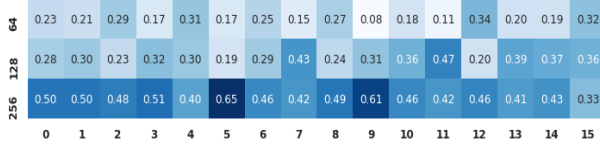


Figure 5: **The feature-wise weights from fine features for proposal corner feature.** We analyze the weights from our model with the input is 256×256 . The darker the color, the larger the proportion of the corresponding scale feature.

1) endpoint representations have more explicit semantic information, especially in edges, and can promote the corner detection model to learn fine grained structure; 2) It is sufficient for our task to adopt vanilla convolution for proposal feature extraction compared to deformable convolution with minor improvements at the cost of extra 10 hours’ training; 3) We train the same epochs for the cross-attention layer but we found that the deformable cross-attention module is much more effective than the cross-attention module; 4) At the same time, the proposal feature enhanced by self-attention can further extract effective information from the fine features. It should be noted that L_{edge} is adopted for different types of cross-attention layer alone when the query embedding is position embedding and L_{boost} for self-attention layer.

Figure 5 visualizes the feature-wise weights in different scale feature maps, which is learned after the normalization of multi-scale fine features in Eq. 4. For the convenience of the display, we merge the total 128-dims corner feature into 16-dims. It can be seen that the weights learned from different scales are 1:1:2 generally, which proves that the feature in a larger scale is more beneficial for edge prediction.

Vertical ablation experiments: We explore each component in CornerFormer through the ablation experiment in Table 3. Corner feature comes from learnable corner feature extractor and position embedding instead if not. Experiment results show that the performance of corner feature is significantly by employing L_{boost} . Direction corner alone is effective for corner detection and performs better with the guidance of L_{seg} . We analyze that the L_{seg} can fur-

Table 3: **The ablation of each component in CornerFormer.** The evaluation metric is the scores of corner/edge/region F-1. $L_{boost}, L_{direct}, L_{seg}$ are the loss functions adopted by our method respectively. Corner Feature with L_{boost} denotes the selected method for edge prediction (The bold one in Table 2).

Corner Feature	L_{boost}	L_{direct}	L_{seg}	Corner	Edge	Region
				86.9	75.1	64.3
		✓		87.7	76.7	66.5
✓				87.6	76.4	68.3
✓	✓			87.7	76.9	70.8
✓	✓		✓	87.8	77.5	70.2
✓	✓	✓		88.2	78.0	71.4
✓	✓	✓	✓	89.0	79.2	71.9

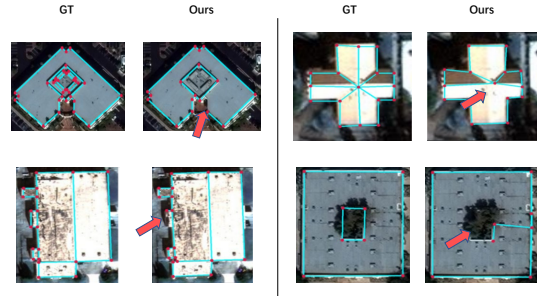


Figure 6: **The failure cases.** The two cases on the left are due to the lack of corners proposed by corner detection and the other two on the right are due to the inconspicuous image signal in the outdoor structure.

ther mine the geometric construction in the image to assist direction corner and transfer more semantic information to edge prediction.

Limitations: The classical failure cases from ours are shown in Fig.6. Although we have been trying to keep the two-stage model in sync, the model based on the bottom-up architecture itself causes edge prediction to be subject to corner detection. Only the proposed corners can be connected as the candidates for edge prediction (e.g., two cases on the left). For areas where the image signal is weak, our model cannot be supplemented with logical reasoning like humans

(*e.g.*, two cases on the right).

5 Conclusion

This paper presents a query-based transformer framework via proposal feature as query embedding for structured reconstruction. Our approach not only facilitates the accurate recall of corners but also demonstrates the necessity of learning large-size features for fine-grained structural reconstruction tasks. More fine structures in the image can be perceived by proposed fine features. We expect this approach to be applied in more areas.

References

- [1] David Acuna, Huan Ling, Amlan Kar, and Sanja Fidler. Efficient interactive annotation of segmentation datasets with polygon-rnn++. In *Proceedings of the IEEE conference on Computer Vision and Pattern Recognition*, pages 859–868, 2018. 2
- [2] Stan Birchfield and Carlo Tomasi. Multiway cut for stereo and motion with slanted surfaces. In *Proceedings of the seventh IEEE international conference on computer vision*, volume 1, pages 489–495. IEEE, 1999. 1
- [3] Ricardo Cabral and Yasutaka Furukawa. Piecewise planar and compact floorplan reconstruction from images. In *2014 IEEE Conference on Computer Vision and Pattern Recognition (CVPR)*, pages 628–635. IEEE, 2014. 2
- [4] Nicolas Carion, Francisco Massa, Gabriel Synnaeve, Nicolas Usunier, Alexander Kirillov, and Sergey Zagoruyko. End-to-end object detection with transformers. *ArXiv*, abs/2005.12872, 2020. 3, 5, 6, 7
- [5] Lluís Castrejon, Kaustav Kundu, Raquel Urtasun, and Sanja Fidler. Annotating object instances with a polygon-rnn. In *Proceedings of the IEEE conference on computer vision and pattern recognition*, pages 5230–5238, 2017. 2
- [6] Jiacheng Chen, Chen Liu, Jiaye Wu, and Yasutaka Furukawa. Floor-sp: Inverse cad for floorplans by sequential room-wise shortest path. *2019 IEEE/CVF International Conference on Computer Vision (ICCV)*, pages 2661–2670, 2019. 1, 2
- [7] Jiacheng Chen, Yiming Qian, and Yasutaka Furukawa. Heat: Holistic edge attention transformer for structured reconstruction. *2022 IEEE/CVF Conference on Computer Vision and Pattern Recognition (CVPR)*, pages 3856–3865, 2022. 2, 4, 5, 6, 7, 8
- [8] Yasutaka Furukawa, Brian Curless, Steven M Seitz, and Richard Szeliski. Manhattan-world stereo. In *2009 IEEE Conference on Computer Vision and Pattern Recognition*, pages 1422–1429. IEEE, 2009. 1
- [9] David Gallup, Jan-Michael Frahm, and Marc Pollefeys. Piecewise planar and non-planar stereo for urban scene reconstruction. In *2010 IEEE computer society conference on computer vision and pattern recognition*, pages 1418–1425. IEEE, 2010. 1
- [10] Kaiming He, Georgia Gkioxari, Piotr Dollár, and Ross B. Girshick. Mask r-cnn. *IEEE Transactions on Pattern Analysis and Machine Intelligence*, 42:386–397, 2020. 2
- [11] Kaiming He, X. Zhang, Shaoqing Ren, and Jian Sun. Deep residual learning for image recognition. *2016 IEEE Conference on Computer Vision and Pattern Recognition (CVPR)*, pages 770–778, 2016. 4
- [12] Varsha Hedau, Derek Hoiem, and David Forsyth. Recovering the spatial layout of cluttered rooms. In *2009 IEEE 12th international conference on computer vision (ICCV)*, pages 1849–1856. IEEE, 2009. 2
- [13] Kun Huang, Yifan Wang, Zihan Zhou, Tianjiao Ding, Shenghua Gao, and Yi Ma. Learning to parse wireframes in images of man-made environments. In *Proceedings of the IEEE Conference on Computer Vision and Pattern Recognition*, pages 626–635, 2018. 3
- [14] Diederik P. Kingma and Jimmy Ba. Adam: A method for stochastic optimization. *CoRR*, abs/1412.6980, 2015. 7
- [15] Jiefeng Li, Siyuan Bian, Ailing Zeng, Can Wang, Bo Pang, Wentao Liu, and Cewu Lu. Human pose regression with residual log-likelihood estimation. In *Proceedings of the IEEE/CVF International Conference on Computer Vision*, pages 11025–11034, 2021. 3
- [16] Jiefeng Li, Tong Chen, Ruiqi Shi, Yujing Lou, Yong-Lu Li, and Cewu Lu. Localization with sampling-argmax. *Advances in Neural Information Processing Systems*, 34:27236–27248, 2021. 2, 3
- [17] Chen Liu, Jiajun Wu, Pushmeet Kohli, and Yasutaka Furukawa. Raster-to-vector: Revisiting floorplan transformation. In *Proceedings of the IEEE International Conference on Computer Vision (ICCV)*, pages 2195–2203, 2017. 3
- [18] Shilong Liu, Feng Li, Hao Zhang, Xiao Yang, Xianbiao Qi, Hang Su, Jun Zhu, and Lei Zhang. Dab-detr: Dynamic anchor boxes are better queries for detr. *arXiv preprint arXiv:2201.12329*, 2022. 3
- [19] Diogo C Luvizon, David Picard, and Hedi Tabia. 2d/3d pose estimation and action recognition using multitask deep learning. In *Proceedings of the IEEE conference on computer vision and pattern recognition*, pages 5137–5146, 2018. 3
- [20] Depu Meng, Xiaokang Chen, ZeJia Fan, Gang Zeng, Houqiang Li, Yuhui Yuan, Lei Sun, and Jingdong Wang. Conditional detr for fast training convergence. In *Proceedings of the IEEE/CVF International Conference on Computer Vision*, pages 3651–3660, 2021. 3
- [21] MS Morley, RM Atkinson, DA Savić, and GA Walters. Ganet: genetic algorithm platform for pipe

- network optimisation. *Advances in engineering software*, 32(6):467–475, 2001. 3, 5
- [22] Nelson Nauata and Yasutaka Furukawa. Vectorizing world buildings: Planar graph reconstruction by primitive detection and relationship inference. In *ECCV*, 2020. 2, 3, 7, 8
- [23] Alejandro Newell, Kaiyu Yang, and Jia Deng. Stacked hourglass networks for human pose estimation. In *European conference on computer vision*, pages 483–499. Springer, 2016. 5
- [24] Shaoqing Ren, Kaiming He, Ross Girshick, and Jian Sun. Faster r-cnn: Towards real-time object detection with region proposal networks. *Advances in neural information processing systems (NeurIPS)*, 28:91–99, 2015. 2
- [25] Sinisa Stekovic, Mahdi Rad, Friedrich Fraundorfer, and Vincent Lepetit. Montefloor: Extending mcts for reconstructing accurate large-scale floor plans. *2021 IEEE/CVF International Conference on Computer Vision (ICCV)*, 2021. 1, 2
- [26] Jonathan J Tompson, Arjun Jain, Yann LeCun, and Christoph Bregler. Joint training of a convolutional network and a graphical model for human pose estimation. *Advances in neural information processing systems*, 27, 2014. 3
- [27] Ashish Vaswani, Noam Shazeer, Niki Parmar, Jakob Uszkoreit, Llion Jones, Aidan N. Gomez, Lukasz Kaiser, and Illia Polosukhin. Attention is all you need. In *NeurIPS*, 2017. 3, 6
- [28] Shih-En Wei, Varun Ramakrishna, Takeo Kanade, and Yaser Sheikh. Convolutional pose machines. In *Proceedings of the IEEE conference on Computer Vision and Pattern Recognition*, pages 4724–4732, 2016. 3
- [29] Yifan Xu, Weijian Xu, David Cheung, and Zhuowen Tu. Line segment detection using transformers without edges. In *CVPR*, 2021. 2, 3, 7, 8
- [30] Nan Xue, Tianfu Wu, Song Bai, Fudong Wang, Guisong Xia, Liangpei Zhang, and Philip H. S. Torr. Holistically-attracted wireframe parsing. *2020 IEEE/CVF Conference on Computer Vision and Pattern Recognition (CVPR)*, pages 2785–2794, 2020. 2, 3, 7, 8
- [31] Changqian Yu, Bin Xiao, Changxin Gao, Lu Yuan, Lei Zhang, Nong Sang, and Jingdong Wang. Litehrnet: A lightweight high-resolution network. In *Proceedings of the IEEE/CVF Conference on Computer Vision and Pattern Recognition*, pages 10440–10450, 2021. 3
- [32] Fuyang Zhang, Nelson Nauata, and Yasutaka Furukawa. Conv-mpn: Convolutional message passing neural network for structured outdoor architecture reconstruction. *2020 IEEE/CVF Conference on Computer Vision and Pattern Recognition (CVPR)*, pages 2795–2804, 2020. 2, 3, 7, 8
- [33] Fuyang Zhang, Xiang Xu, Nelson Nauata, and Yasutaka Furukawa. Structured outdoor architecture reconstruction by exploration and classification. In *Proceedings of the IEEE/CVF International Conference on Computer Vision*, pages 12427–12435, 2021. 2, 7, 8
- [34] Hao Zhang, Feng Li, Shilong Liu, Lei Zhang, Hang Su, Jun Zhu, Lionel M Ni, and Heung-Yeung Shum. Dino: Detr with improved denoising anchor boxes for end-to-end object detection. *arXiv preprint arXiv:2203.03605*, 2022. 3
- [35] Ziheng Zhang, Zhengxin Li, Ning Bi, Jia Zheng, Jinlei Wang, Kun Huang, Weixin Luo, Yanyu Xu, and Shenghua Gao. Ppgnet: Learning point-pair graph for line segment detection. In *Proceedings of the IEEE/CVF Conference on Computer Vision and Pattern Recognition (CVPR)*, pages 7105–7114, 2019. 2
- [36] Yichao Zhou, Haozhi Qi, and Yi Ma. End-to-end wireframe parsing. In *Proceedings of the IEEE/CVF International Conference on Computer Vision*, pages 962–971, 2019. 2, 3
- [37] Yichao Zhou, Haozhi Qi, and Yi Ma. End-to-end wireframe parsing. *2019 IEEE/CVF International Conference on Computer Vision (ICCV)*, pages 962–971, 2019. 3
- [38] Zixiang Zhou, Xiangchen Zhao, Yu Wang, Panqu Wang, and Hassan Foroosh. Centerformer: Center-based transformer for 3d object detection. *arXiv preprint arXiv:2209.05588*, 2022. 2, 6, 9
- [39] Xizhou Zhu, Weijie Su, Lewei Lu, Bin Li, Xiaogang Wang, and Jifeng Dai. Deformable detr: Deformable transformers for end-to-end object detection. *ArXiv*, abs/2010.04159, 2021. 3, 4